New Universal Figure of Merit for Embedded Si Piezoresistive Pressure Sensors

Thibault P. Delhaye, *Student Member, IEEE*, Nicolas André *Member, IEEE*, Laurent A. Francis, *Member, IEEE*, and Denis Flandre, *Senior Member, IEEE*

***Abstract*— In this paper, we are presenting a new classification methodology for high resolution membrane based MEMS piezoresistive pressure sensors embedded in Internet of Things (IoT) nodes or in body-implanted devices. This is based on a new figure of merit (FoM) that includes the four key parameters as the power consumption, the area, the noise and the sensitivity of the transducer. The proposed classification allows to directly evaluate, based on power consumption and area requirements, the ultimate limit of detection that can be reached by a proposed technology. The derivation of the proposed FoM is validated based on wide survey and comparisons of literature results. It shows that, until now, wet etching technics for membrane release still allow for reaching higher performances than reactive ion etching.**

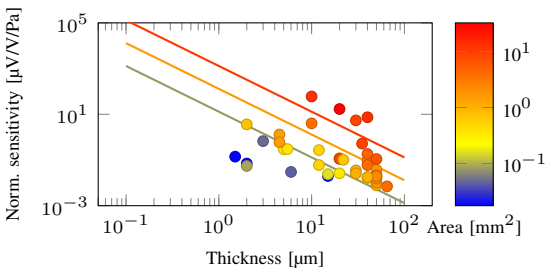

***Index Terms*— Piezoresistive Pressure Sensor, MEMS, Figure of Merit.**

I. Introduction

Silicon-based piezoresistive pressure sensors are a well-known mature technology. Since 1950's, these sensors have been developed and improved, thanks to better understanding of silicon piezoresistivity, new fabrication techniques, and new simulation tools that allows for reaching better performance by optimization of the shape of the membrane and of its constitutive materials. Multiple figures of merit exist, including sensitivity, linearity over a given range and signal-to-noise ratio. These classical FoM are not sufficient anymore due to the emergence of the Internet of Things nodes or in body-implanted devices that require sensors with extremely low power consumption, under hundreds of microWatts as well as small size, as small as a fraction of millimeter square. For example, intraocular pressure or blood pressure monitoring requires implanted pressure sensors smaller than 2 $[mm^3]$, achieving at least 100 $[Pa]$ resolution and consuming less than 100 $[\mu W]$ [1] [2]. Some researches have already begun to consider these constraints by using MOSFET as sensing elements to lower the power consumption [3] [4].

Usually, the selection of a sensor has to be made based on the required specifications that lead to one kind of technology or another. But how to evaluate and make certain that keeping the same sensor topology and just changing its size or its bias condition will lead to a better solution that the ones that are currently provided? Indeed, neither power supply nor the die area are technology dependent and it could be interesting to have a FoM related to the intrinsic performance of a technology that could be valid inside a certain range of power supply and membrane size.

In this paper, we will first introduce the classical architecture of the piezoresistive pressure sensors, then we will present all the basics to understand the behavior of these sensors and derive the useful equations to build a simple theoretical model. Then we will build a new figure of merit to identify topologies of interest, focusing on IoT nodes applications that require very small size and very low power consumption. Finally, we will present a wide survey of the literature and compare its results thanks to the classical and our new FoM.

II. Classical Topology of Piezoresistive Pressure Sensor

Pressure sensors based on piezoresistive strain gauges are indirect transducers that firstly convert a pressure variation to a mechanical strain variation that secondly is transmitted to the silicon strain gauges yielding an electrical signal. The classical structure of silicon piezoresistive pressure sensors is based on doped (around $10^{17}[cm^{-3}]$) resistors, called piezoresistors, as strain gauges embedded on a thin silicon, or silicon dioxide, membrane on which is applied a difference of pressure causing stress on his edge, where the membrane is anchored to the substrate. As can be seen on fig.1, the piezoresistors, in red, are located at these specific points on the membrane, in blue, where the strain/stress is maximum.

The membrane is released by etching of the silicon substrate, in yellow. In the past years, these membranes could either be thin (about 1 µm) with small area, thanks to surface

This work was supported by a FRIA fellowship from the F.R.S.-FNRS, Belgium.

T. P. Delhaye, N. André, L.A. Francis and D. Flandre are with the Institute of Information and Communication Technologies, Electronics and Applied Mathematics (ICTEAM), UCLouvain, Louvain-la-Neuve, 1348, Belgium (e-mail: thibault.delhaye@uclouvain.be).

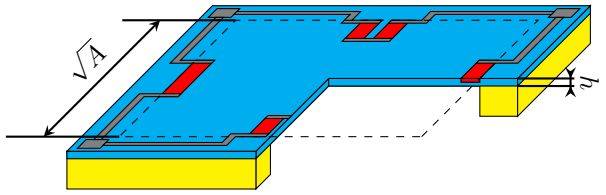

Fig. 1. Cross-section view of a typical piezoresistive pressure sensor: silicon handle wafer is in yellow, silicon or silicon dioxide membrane of thickness $\boldsymbol{h}$ and area $\boldsymbol{A}$ is in blue, piezoresistors are in red and aluminum conductive lines are in gray, dashed lines delimit the membrane.

micro-machining, or thick (more than 10 µm) with large area, thank to bulk-micro-machining. More recently, with the advent of the Silicon-On-Insulator (SOI) technology, producing thin membranes with large area has become possible by using the buried oxide (BOX) as an accurate etch-stop layer.

The dimensions of the membrane are denoted h for the thickness and A for the area.

About the etching process, silicon wet etching with KOH or TMAH is the fastest and easiest process but allows only sides in [110] silicon orientation, leading to square or rectangular uniform shapes. Silicon dry etching by Deep Reactive Ion Etching (DRIE), e.g. Bosch process, takes more time and resources but allows to achieve more complex shapes for enhancing the sensitivity thanks to the use of membrane patterning, e.g. letting an island of silicon above or below the dioxide membrane. But using thin membranes has some drawbacks: it is more complex to fabricate, and process yield is smaller.

Concerning the electrical readout, a classic implementation to monitor resistance variation is the Wheatstone bridge. In this case four spots where stresses are concentrated can be used to obtain a full-bridge configuration as represented in fig. 2.

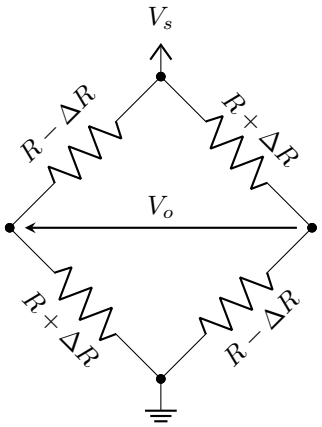

Fig. 2. Classical Wheatstone full-bridge structure. $\boldsymbol{V_s}$ is the supply voltage, $\boldsymbol{V_o}$ the output signal depending on the resistance variation $\boldsymbol{\Delta R}$ of the resistors.

III. Piezoresistive Pressure Sensor Basics

A. Piezoresistivity

The strain gauges are typically made of deposited and patterned doped polysilicon or monocrystalline silicon resistors realized by implantation in bulk Si or in SOI layers. They can be highly or lightly p- or n-type doped. The aim of doping silicon is to enhance its conductivity in order to achieve a predictive resistive behavior, to avoid some detrimental space-charge effects, and to provide predictive piezoresistive properties meaning that the silicon conductivity will vary with stress. The capability of a material to change its resistivity regarding to the strain is given by its Gauge Factor (GF) that is the ratio between its relative resistivity change and the strain applied to the resistor. The piezoresistive effect derives from the piezoresistive coefficient matrix, respectively π_p and π_n, that links directional stress to directional change of resistivity relate to crystalline orientation. At standard temperature and doping conditions of respectively 300 K and 10^{16} cm^{-3}, it is written as:

$$\pi_p = \begin{pmatrix} 66 & -11 & -11 & 0 & 0 & 0 \\ -11 & 66 & -11 & 0 & 0 & 0 \\ -11 & -11 & 66 & 0 & 0 & 0 \\ 0 & 0 & 0 & 1381 & 0 & 0 \\ 0 & 0 & 0 & 0 & 1381 & 0 \\ 0 & 0 & 0 & 0 & 0 & 1381 \end{pmatrix} \quad (1)$$

$$\pi_n = \begin{pmatrix} -1022 & 534 & 534 & 0 & 0 & 0 \\ 534 & -1022 & 534 & 0 & 0 & 0 \\ 534 & 534 & -1022 & 0 & 0 & 0 \\ 0 & 0 & 0 & -136 & 0 & 0 \\ 0 & 0 & 0 & 0 & -136 & 0 \\ 0 & 0 & 0 & 0 & 0 & -136 \end{pmatrix} \quad (2)$$

in $[\mathrm{TPa}^{-1}]$ from [5].

P-doped [110] silicon resistors are historically the most used piezoresistors due to the high GF, to the similar magnitude and opposite sign of parallel and perpendicular piezoresistive coefficients, respectively $\pi_{\parallel} = (\pi_{11} + \pi_{12} + \pi_{44})/2 = 718$ [TPa^{-1}] and $\pi_{\perp} = (\pi_{11} + \pi_{12} - \pi_{44})/2 = -663$ [TPa^{-1}] [5], and to the ease of fabrication (membrane release thanks to highly selective and anisotropic wet etching). With new available fabrication techniques it has become possible to achieve shapes that are more complex and the use of n-doped silicon could become interesting.

Variation of the piezoresistive coefficients with the temperature and doping concentration have been experienced. Richter proposed a model that allows to accurately predict the relative values of these piezoresistive coefficient regarding to standard conditions [6]:

$$\pi(N,T) = \frac{\pi(10^{16},300)T_n^{-\theta}}{1 + \left(\frac{N}{N_b}\right)^{\alpha} T_n^{-\beta} + \left(\frac{N}{N_c}\right)^{\gamma} T_n^{-\eta}} \quad (3)$$

with $T_n = T/300$ the normalized temperature, N the doping concentrations and θ, α, β, γ, η, N_b and N_c the fitting parameters whose values are respectively 0.95, 0.39, 1.35, 0.94, 4.55, 4.9×10^{19} and 2.6×10^{20}. Theoretical curves for π_{44} of p-type silicon are presented in fig. 3.

This leads to two conclusions: piezoresistive sensor performances will decrease at high temperature, and it is important to consider doping concentration when designing the sensor.

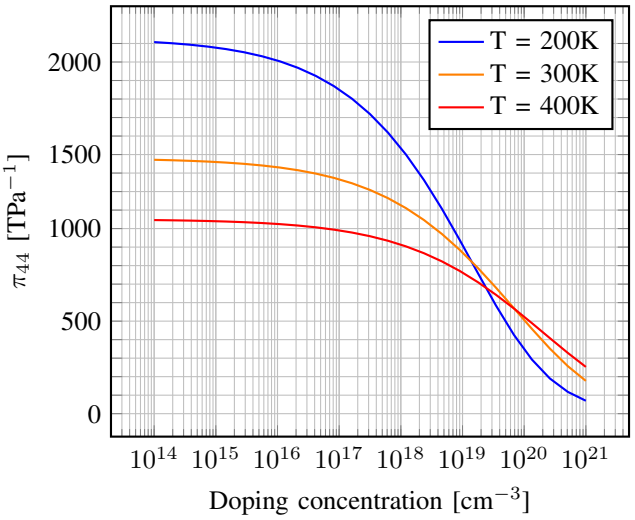

Fig. 3. π_{44} Piezoresistive coefficient of p-doped silicon versus doping concentration and temperature adapted from Doll and Pruitt [7].

B. Wheatstone Bridge as Stress to Voltage Transducer

To evaluate the resistance variation of the piezoresistors, the Wheatstone bridge implementation presents several major advantages. It reduces the zero-pressure offset voltage and then enhances the dynamic range, and it cancels the first-order dependency on temperature. This is a widely used configuration, leading to well documented behavior, readout and compensation possibilities. On the other hand, this is a passive circuit, leaving no degree of freedom once fabricated, leading to a fixed relationship between sensitivity and bias voltage and thus consumption and noise as we will develop below.

Depending on the number of sensitive gauges, from 1 to 4, the bridge is named a quarter-, a half- or a full-bridge respectively. The major differences between each case are a gain of sensitivity from 1 to 4, from the quarter- to the full-bridge and an increase in the linearity of the response for the half- and full-bridge. For these reasons, most of the time the full bridge is preferred.

For the full-bridge presented in fig. 2 the resistors with positive and negative variations can respectively be resistors perpendicular, $R_\perp$, and parallel, $R_\parallel$, to the membrane edges. Their values can be expressed as:

$$\begin{aligned} R_\parallel &= R_0(1 + \pi_\parallel\sigma_\parallel + \pi_\perp\sigma_\perp) \\ R_\perp &= R_0(1 + \pi_\parallel\sigma_\perp + \pi_\perp\sigma_\parallel) \end{aligned} \tag{4}$$

with $\sigma_\parallel$ and $\sigma_\perp$ the stresses appearing in parallel and in perpendicular with the edge of the membrane due to the applied pressure.

Finally, the output voltage, V_o, can be expressed as:

$$V_o = \frac{R_\parallel - R_\perp}{R_\parallel + R_\perp} V_s \tag{5}$$

expressed in [V], as a function of V_s, the supply voltage.

C. Membrane as Pressure to Stress Transducer

For equations (4) and (5), stresses applied to the resistors are needed to know the output voltage. A simple model to predict the value of these stresses is based on a simple and uniform silicon membrane of thickness h and area A for which the stresses in the middle of the edges can be expressed as [8]:

$$\begin{aligned} \sigma_\perp &= 0.25\frac{A}{h^2}p \\ \sigma_\parallel &= 0.25\frac{\nu A}{h^2}p \end{aligned} \tag{6}$$

expressed in [N/m^2], with ν the silicon Poisson's ratio and p the applied pressure on the membrane in [Pa].

D. Sensitivity

The sensitivity of the system is defined as the slope of the relationship between the output signal and the pressure applied on the system. It can be written as the product of mechanical sensitivity, which is linked to the membrane characteristics (its materials and its topology), the piezoresisitive effect, which is linked to the resistors material and positions on the membrane, and the electrical sensitivity that is linked to the circuit used, here Wheatstone bridge.

Using equations (4), (5) and (6), the output voltage versus pressure relationship can be written as:

$$V_o = \frac{p\left[\left(\pi_\parallel + \nu\pi_\perp\right) - \left(\nu\pi_\parallel + \pi_\perp\right)\right] 0.25\frac{A}{h^2}}{2 + p\left((1+\nu)\left(\pi_\parallel + \pi_\perp\right)\right) 0.25\frac{A}{h^2}} V_s \tag{7}$$

and the sensitivity, assuming that the changes introduced by the pressure are small, is computed as:

$$S = \frac{\partial V_o}{\partial p} = \frac{(1-\nu)(\pi_\parallel - \pi_\perp)}{2} 0.25\frac{A}{h^2} V_s \tag{8}$$

usually expressed in [µV/Pa].

Sensitivity is a crucial parameter of a sensor because it will lead to a limitation in resolution, depending on the readout circuit, and a need of amplification if the sensitivity is too low. A classical way to express sensitivity for piezoresistive pressure sensors is the normalized sensitivity to bias voltage ratio, leading to:

$$\frac{\partial V_o/V_s}{\partial p} = \frac{(1-\nu)(\pi_\parallel - \pi_\perp)}{2} 0.25\frac{A}{h^2} \tag{9}$$

usually expressed in [µV/V/Pa].

E. Noise

Electronic noise appears as tiny random fluctuations of voltage and current that are induced by all elements of an electronic circuit and that affect the signal that is read at the output of the sensor. There are two main sources of noise in silicon resistors: the thermal noise and the flicker noise. The thermal noise, whose spectral density is denoted S_{th}, is related to the temperature and the bridge equivalent resistance, which is equal to R, according to [9]:

$$S_{th} = 4k_bTR \tag{10}$$

expressed in [V^2/Hz].

The flicker noise, $S_{1/f}$, is related to the number of carriers,N_c, the bias voltage, the frequency and a undimensional technology coefficient, α, whose value usually lies between 10^{-4} and 10^{-7} and that is related to the number of defects in the device [10], according to:

$$S_{1/f} = \frac{\alpha V_s^2}{N_c f} \tag{11}$$

F. Limit of detection

The limit of detection (LoD) is defined as [11]:

$$LoD = 3\frac{N}{S} \tag{12}$$

where N is the standard deviation of the output signal with a constant pressure input, and S the sensor sensitivity. This is the minimum change of pressure that induces a measurable variation of the output signal, i.e. the minimum pressure signal that allows for reaching a signal-to-noise ratio (SNR) higher than 10 dB.

We assume that flicker and thermal noises dominate in the considered bandwidth which is defined between $1[Hz]$ and B, that is usually much more bigger than $1[Hz]$. We use the expression of the sensitivity (8) to define the limit of detection of a pressure sensor made of a simple and uniform silicon membrane with four piezoresistors placed in the middle of the membrane edges :

$$\begin{aligned} LoD &= 3\frac{\sqrt{\int_1^B (S_{th} + S_{1/f})df}}{\frac{\partial V_o}{\partial p}} \\ LoD &= 3\frac{\sqrt{4k_bTRB + \frac{\alpha V_s^2}{N_c}\log(B)}\ 8h^2}{(1-\nu)(\pi_{\parallel} - \pi_{\perp})AV_s} \end{aligned} \tag{13}$$

expressed in [Pa].

IV. Figures of Merit

At this stage, we built a simple theoretical model showing that to have a high resolution, it is important to have a high ratio between sensitivity and the square-root of the noise. For traditional pressure sensors, the LoD, is an efficient way to present the capability of a sensor to yield an information with a known uncertainty, regardless of the power consumption, that is rather low, typically some milliWatts, and whatever the size of the sensor, that is rather low as well, typically some millimeters-square. But this is no longer applicable for pressure sensors embedded in IoT nodes or implanted devices : only few tens of microWatts and a fraction of millimeters-square is left for sensors. We need to include the power consumption and the area in the figures of merit.

To define the new FoM, we consider that by meaning over k samples of a Gaussian random signal, and so by increasing the energy used for the measurement by k, the error is decreased by $\sqrt{k}$. This means that an increase of power by a factor k needs to reduce the LoD by a factor bigger than $\sqrt{k}$ to be energy effective. In the same way, if the membrane is modeled as a perfect spring, an increase of area by a factor k leads to an increase of signal power of k^2. So this means that an increase of the area by a factor k needs to reduce the LoD by a factor bigger than k to be area effective. Finally, by considering that LoD is the resolution of the transducer, its inverse value expresses the most efficient number of digital bits to use considering the desired range of the sensor.

Then we see that a new quantity that characterizes the resolution achievable by a technology depending on the area and the power available for the sensor can be obtained. This is computed by inverting the LoD multiplied by the area and the square-root of the power:

$$FoM = \left(LoD.\sqrt{P}.A\right)^{-1} \tag{14}$$

expressed in [$Pa^{-1}.\mu W^{-1/2}.mm^{-2}$] and that needs to be maximized. All the parameters needed to compute this FoM can directly be measured on existing sensors.

This FoM is then subdivided into a mechanical FoM and an electrical FoM as follows:

$$FoM = \frac{V_s}{3N\sqrt{P}}.\frac{S}{V_s A} = FoM_e.FoM_m \tag{15}$$

For our simple theoretical model, these three FoM can be expressed as :

$$\begin{aligned} FoM &= \frac{\sqrt{R}(1-\nu)(\pi_{\parallel} - \pi_{\perp})}{3\sqrt{4k_bTRB + \frac{\alpha V_s^2}{N_c}\log(B)}8h^2} \\ FoM_e &= \frac{\sqrt{R}}{3\sqrt{4k_bTRB + \frac{\alpha V_s^2}{N_c}\log(B)}} \\ FoM_m &= \frac{(1-\nu)(\pi_{\parallel} - \pi_{\perp})}{8h^2} \end{aligned} \tag{16}$$

V. State of the Art Analysis

As discussed above, the most common figure of merit for micro-machined pressure sensor is the sensitivity, or the sensitivity normalized to the voltage supply, but as it can be seen in Table I, sensors with comparable sensitivity can have either really different sizes (e.g. [12] compared to [13]), or consume a lot more power (e.g. [12] compared to [14]). These differences can have multiple sources, as for example: (i) different doping concentrations, that can play a role in piezoresistivity, (ii) topological optimizations, that allows for concentrating stresses on the piezoresistors, or (iii) the dimensions of the piezoresistors. These parameters are crucial for IoT nodes or implantable devices, that need to consume extremely low power and be as small as possible.

Another figure of merit that is more rarely considered is the output noise. However this value is crucial to reach a targeted resolution. Mitigating a high noise value thanks to a high resolution ADC and averaging will lead to high power consumption, waste of memory and conversion time. Moreover, considering only sensitivity regardless of an increase in output noise can lead to useless complex designs that do not lead to an increased resolution.

TABLE I
PIEZORESISTIVE PRESSURE SENSOR WITH VOLTAGE OUTPUT COMPARISON.

Ref	Year	A [mm²]	h [µm]	Norm. Sens. [µV/V/Pa]	Range [kPa]	V_s [V]	Current [mA]	Resist. [kΩ]	P [mW]	Doping $[cm^{-3}]$	N [µV]	Technology
[15]	1985	1	30	0.035	200	10				3×10^{18}		mono-Si
[12]	1991	0.41	5	0.3	93.32	5		0.46	54.3	3×10^{18}		mono-Si
[13]	1995	0.64	20	0.12	88.2	7				5×10^{17}		mono-Si
[14]	1996	0.36	5.5	0.3	200	5		2.8	8.9	2.50×10^{18}		mono-Si
[16]	1996	0.02	1.5	0.14	50	2.5		3	2.08		60	p-Si
[16]	1996	0.02	2	0.07	50	2.5		3	2.08		10	p-Si
[17]	2003	9	20	0.1116	20		1	4.48	4.48	2×10^{20}		p-Si
[18]	2004	0.49	40	0.016	100	5				5×10^{17}		mono-Si
[18]	2004	2.89	40	0.095	100	5				5×10^{17}		mono-Si
[18]	2004	4.84	40	0.183	100	5				5×10^{17}		mono-Si
[19]	2006	0.5	12	0.06	800	10						p-Si
[19]	2006	0.5	12	0.27	800	10						p-Si
[20]	2006		15	0.02	1000	10		1	100			p-Si
[21]	2011	0.36	20	0.026	750	3.3		3	3.63	1×10^{19}	12.87	mono-Si
[22]	2013	0.16	15	0.024	700		1	5	5	2×10^{18}		mono-Si
[23]	2014	4	40	0.06	106	3						mono-Si
[24]	2014	0.05	3	0.67		0.5				3×10^{18}		mono-Si
[25]	2014	3.61	10	4	0.005			3.9		2.50×10^{18}		mono-Si w/ concentrators
[26]	2015	4	65	0.007	413.7	3.3		3.6	3			p-Si
[27]	2015	0.045	6	0.03	2500	5						p-Si
[28]	2015	0.09	35	0.52	100	5						p-Si
[29]	2015	1.69	50	0.037		3.3		11	0.99			mono-Si
[30]	2015	5.76	50	0.11	138	9	1.5	5.8	13.96	1.60×10^{20}	122	mono-Si
[31]	2015	0.64	22	0.102	30	5						mono-Si
[32]	2015	1	30	0.026	300	5		5	5	3×10^{18}		mono-Si
[33]	2016	1.12	50	0.0078	3000	3.3		11	0.99			p-Si
[33]	2016	1.64	50	0.0102	3000	3.3		11	0.99			p-Si
[33]	2016	2.19	50	0.0193	3000	3.3		11	0.99			p-Si
[33]	2016	2.86	50	0.0218	3000	3.3		11	0.99			p-Si
[34]	2016	0.09	2	0.0548	100	1		2.34	0.43			p-Si
[35]	2016	2.19	50	0.0153	3000	3.3		11	0.99			p-Si
[35]	2016	2.19	50	0.0193	3000	3.3		11	0.99			p-Si
[36]	2016	32.49	20	17	0.5	5		100	0.25	3×10^{14}	1147	mono-Si w/ concentrators
[37]	2016	1	40	0.018	1000	5		5	5	3×10^{17}		mono-Si
[38]	2017	0.71	2	3.6	1.2	5		3	8.3		10	mono-Si w/ concentrators
[39]	2017	12.25	10	60	0.5	5		3.8	6.58		900	mono-Si w/ concentrators
[40]	2018	8.41	30	5.4	5	5		4.5	5.55	3.50×10^{17}		mono-Si w/ concentrators
[41]	2018	12.96	40	7.4	6.9	5		6.7	3.73		765	mono-Si w/ concentrators
[4]	2019	1.44	4.5	1.3		5	0.038		0.19			mono-Si
[4]	2019	1.44	4.5	0.6		5	0.079		0.395			mono-Si

The conclusion of this State of the Art review is that even if an impressive increase in sensitivity has been achieved over the years, the emphasis on power consumption, size and resolution is currently not sufficient to allow for evaluating the real performances of sensors designed to be embedded in an IoT nodes.

A. Normalized Sensitivity

Fig.4 presents a comparison between normalized sensitivities extracted from Table I, without any classification regarding to the used technology, the thickness or the area of the membrane. As predicted by theoretical trends (solid lines), it can be seen that the thinner the membrane, and the wider the area, the greater is the sensitivity. The three theoretical lines, corresponding to our simple uniform mono-Si model, are showing a slight difference with the performances presented in Table I. We can see that the theoretical model seems to overestimate the sensitivity of small-size membranes and underestimate the sensitivity of large-size membranes: Small membranes can be impacted by the size of the piezoresistors that become too large to be only influenced by the highest stresses, while large membranes enable the use of stress concentrators that enhance their response.

B. Mechanical Figure of Merit

Fig.5 shows the comparison of the sensors of the state of the art regarding the Mechanical FoM, presented in section IV, in which the effect of the area is mitigated. We can clearly see the effect of the thickness of the membrane, that allows for improving the sensitivity without any area increase. Moreover, three main groups of sensors can be highlighted: the sensors using poly-Si are presented in red, mono-Si in blue and mono-Si with stress concentrators are presented in black. As we can see, poly-Si based sensors show slightly smaller sensitivity than mono-Si based sensors, due to their smaller piezoresistive coefficient ($\pi_{\parallel} = 588[TPa^{-1}]$ and $\pi_{\perp} = -185[TPa^{-1}]$ for poly-Si [42] since $\pi_{\parallel} = 718[TPa^{-1}]$ and $\pi_{\perp} = -663[TPa^{-1}]$ for mono-Si [5]) and sensors with stress-concentrators show highest sensitivities related to their thickness. The theoretical line of our model has also been

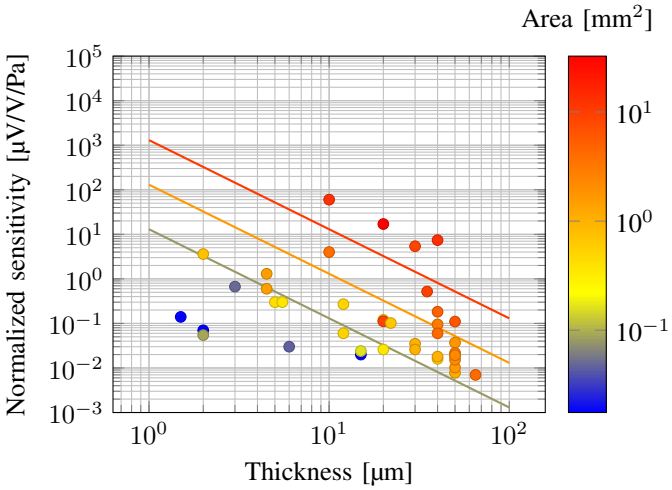

Fig. 4. Normalized sensitivity versus membrane thickness (x-axis) and membrane area (color circles). Lines are theoretical trends obtained with the simple model, eq. (9), for areas of 0.1, 1 and 10 mm^2, from bottom to top.

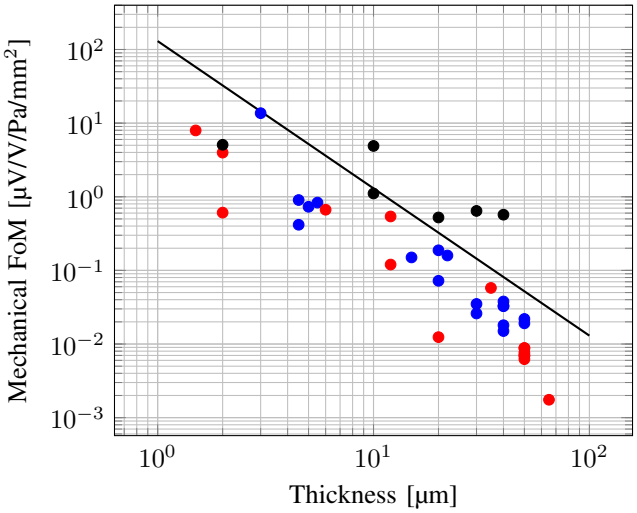

Fig. 5. Mechanical FoM versus membrane thickness. Color dots indicate the technology used: red = polysilicon; blue = monocrystalline silicon; black = monocrystalline silicon with stress concentrators. Black line is the theoretical trend of the simple model, eq. (16).

added, confirming the trends and showing a strong interest for stress concentrators even if their influence seems to be reduced when membranes size become small.

Thanks to FoMm we show that stress concentrators allow for improving normalized sensitivity of pressure sensor using area effectively.

C. Electrical Figure of Merit

Fig. 6 shows state of the art sensors comparison regarding the noise normalized to the bias voltage. This FoM is more difficult to evaluate because only few papers give information about noise analysis of the output signal. To illustrate the theoretical trend that should be followed, we added a line showing how the FoMe of a $20[k\Omega]$ resistance Wheatstone bridge, with p-doped ($10^{-17}[cm^{-3}]$), $100[nm]$ thick, $5[\mu m]$

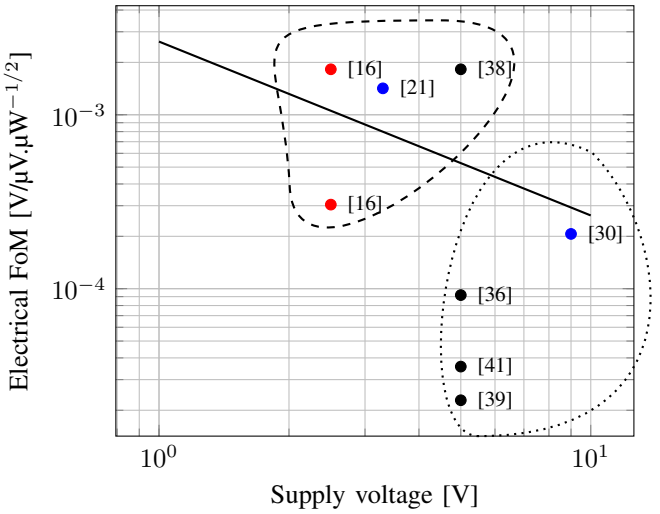

Fig. 6. Electrical FoM versus supply votlage. Color dots indicate the technology used: red = polysilicon; blue = monocrystalline silicon; black = monocrystalline silicon with stress concentrators. The dashed and dotted lines enclose respectively the membranes released by TMAH and DRIE. Black line is the theoretical trend of the simple model, eq. (16).

wide and $6.4[\mu m]$ long, piezoresistors, with a technology coefficient α equal to 10^{-4}, should change with supply voltage, considering a $10[kHz]$ bandwith.

Two groups of sensors can be differentiated: a first one is the group of small-area sensors, released by TMAH wet etching [16] [21] [38], and a second one is the group of large-area sensors, in this case released by DRIE [30] [36] [39] [41] [43]. It has been demonstrated that a mechanical source of noise (e.g. Brownian motion) has a lower impact than the electrical sources of noise [44]. So the additionnal sources of noises in DRIE sensors should probably result from the trapped charges induced by reactive ion etching, also creating space-charge effects [45]. Poly-Si sensors also seem to show higher noise at the output than mono-Si which can be expected from the defects present in polysilicon at the grain boundaries or at the a polysilicon / insulator interface. The whole goal of using DRIE for larger membrane is nevertheless to produce specific shapes that will allow to compensate the normalized noise by an area trade-off and by drastically increasing the sensitivity of the sensor, as discussed next. In-situ thermal annealing could also be used to reduce 1/f noise [46].

Thanks to FoMe, we notice an advantage of small membranes released by wet etching. We also highlighted the need for DRIE to significantly increase the sensitivity of the devices to mitigate noise increase.

D. Limit of Detection

In terms of limit of detection, that is also equal to the ratio between normalized noise and normalized sensitivity, fig. 7 reveals that increasing the size and adding stress concentrators allows for reaching the finest resolutions. For classical applications requiring high resolution, this is the most important figure of merit. But it does not consider the power consumption nor the space required that are two

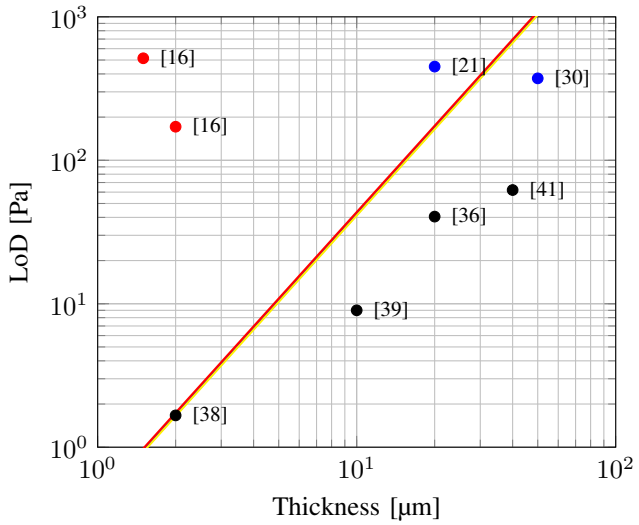

Fig. 7. Limit of Detection versus membrane thickness. Color dots indicate the technology used: red = polysilicon; blue = monocrystalline silicon; black = monocrystalline silicon with stress concentrators. Lines are theoretical trends of the simple model, eq. (13). Colors indicate supply voltage : blue = 1 [V]; yellow = 3.3 [V]; red = 5 [V].

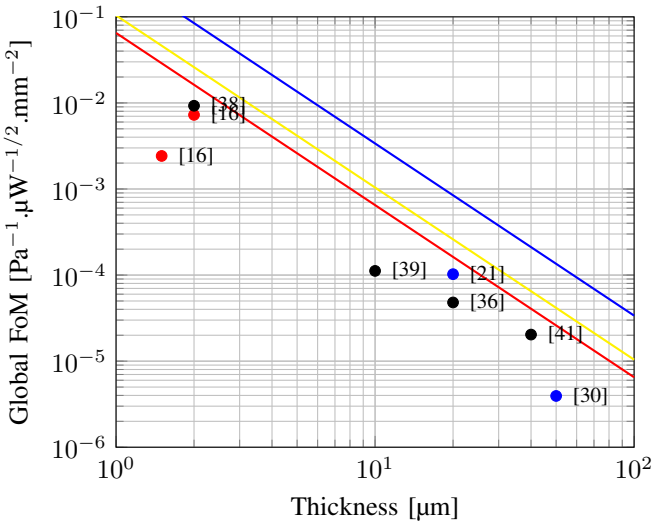

Fig. 8. Global Figure of Merit versus membrane thickness. Colors indicate the technology used: red = polysilicon; blue = monocrystalline silicon; black = monocrystalline silicon with stress concentrators. Lines are theoretical trends of the simple model, eq. (16). Colors indicate supply voltage : blue = 1 [V]; yellow = 3.3 [V]; red = 5 [V].

critical parameters for sensors embedded in IoT nodes or implanted medical devices: LoD is not sufficient anymore. We added theoretical lines representing the simple model, considering a $1[mm^2]$ membrane sensor at different supply voltages, showing that, considering a given technology, sensors of the literature are following the logical trends.

E. Global Figure of Merit

Finally, the new global FoM for the state of the art is depicted in fig.8 and we added lines representing our simple model. We can clearly see that the best values are obtained for the thinnest membranes, following the theoretical trends. Thickness of the membrane being correlated with pressure range, an improvement of the FoM of a sensor, with specific pressure range, is represented as an upward vertical displacement of the point representing the sensor on this graph. This means that an improvement in terms of size, consumption or limit of detection has been efficiently made without impacting significantly the other two parameters.

It can be seen that the gain in sensitivity obtained by using stress concentrators thanks to DRIE process to release the membranes, is not sufficient to compensate the added noise, area and power consumption of these sensors. To the best of our knowledge, it appears that prof. X. Li's group [21] [38] has found the best trade-off allowing for reaching very high resolution while keeping relatively small area (around 1mm^2) by using an innovative smart wet etching on (111) silicon wafer.

Thanks to the global Figure of Merit, the best high resolution, low power and small size sensors are easily highlighted. It appears that sensors with membranes released by wet etching keep staying of high interest especially since wet etching is cheaper, faster and more homogenous than DRIE but letting less freedom for the membrane shape design.

VI. Conclusion

In this paper, key parameters of piezoresistive pressure sensors have been reviewed, by analytical developments and state of the art comparison. More than 30 of the most cited papers of the literature have been analysed. We derived a theoretical model for a simple and uniform Si membrane based pressure sensor and we used classical figures of merit to make a comparison between this model and of the state of the art sensors performances thanks to original graphs showing the different technologies effects.

Then we defined a new universal figure of merit including all classical parameters as noise and sensitivity but also new constraints of crucial importance for new applications in IoT nodes or in body-implanted devices: the power consumption and the area. With this new FoM, interest of membrane patterning is mitigated allowing a boost of sensitivity from a mechanical point of view but leading to an increase of output noise. On the other hand, low sensitivity of small size membranes released by wet etching demonstrate high performances thanks to their low noise generation.

References

[1] G. Chen, H. Ghaed, R.-u. Haque, M. Wieckowski, Y. Kim, G. Kim, D. Fick, D. Kim, M. Seok, K. Wise *et al.*, "A cubic-millimeter energy-autonomous wireless intraocular pressure monitor," in *2011 IEEE International Solid-State Circuits Conference*. IEEE, 2011, pp. 310–312.

[2] N. J. Cleven, J. A. Müntjes, H. Fassbender, U. Urban, M. Görtz, H. Vogt, M. Gräfe, T. Göttsche, T. Penzkofer, T. Schmitz-Rode *et al.*, "A novel fully implantable wireless sensor system for monitoring hypertension patients," *IEEE Transactions on Biomedical Engineering*, vol. 59, no. 11, pp. 3124–3130, 2012.

[3] N. André, T. P. Delhaye, M. Al Kadi Jazairli, B. Olbrechts, P. Gérard, L. A. Francis, J.-P. Raskin, and D. Flandre, "Ultra-low-power soi-cmos pressure sensor based on orthogonal pmos gauges," in *XXII IMEKO TC4 International Symposium and XX International Workshop on ADC Modelling and Testing*, 2017.

[4] E. L. Gardner, A. De Luca, J. Philippe, D. Dragomirescu, and F. Udrea, "Thin-film mosfet-based pressure sensor," *IEEE Sensors Letters*, vol. 3, no. 7, pp. 1–4, Jul. 2019.

[5] C. S. Smith, "Piezoresistance effect in germanium and silicon," *Phys. Rev.*, vol. 94, pp. 42–49, Apr. 1954.

[6] J. Richter, J. Pedersen, M. Brandbyge, E. V. Thomsen, and O. Hansen, "Piezoresistance in p-type silicon revisited," *Journal of Applied Physics*, vol. 104, no. 2, pp. 1–8, Jul. 2008.

[7] J. C. Doll and B. L. Pruitt, "Piezoresistance fundamentals," in *Piezoresistor Design and Applications*, R. T. Howe and A. J. Ricco, Eds. Springer New York, 2013, ch. chapter 2, pp. 21–49.

[8] V. Kaajakari *et al.*, "Practical mems: Design of microsystems, accelerometers, gyroscopes, rf mems, optical mems, and microfluidic systems," *Las Vegas, NV: Small Gear Publishing*, 2009.

[9] H. Nyquist, "Thermal agitation of electric charge in conductors," *Phys. Rev.*, vol. 32, no. 1, p. 110, Jul. 1928.

[10] J. Harley and T. Kenny, "High-sensitivity piezoresistive cantilevers under 1000 å thick," *Appl. Phys. Lett.*, vol. 75, no. 2, pp. 289–291, 1999.

[11] J. E. Knoll, "Estimation of the limit of detection in chromatography," *Journal of Chromatographic Science*, vol. 23, no. 9, pp. 422–425, Sep. 1985.

[12] G.-S. Chung, S. Kawahito, M. Ishida, T. Nakamura, M. Kawashima, and T. Suzaki, "High-performance pressure sensors using double silicon-on-insulator structures," *Review of scientific instruments*, vol. 62, no. 5, pp. 1341–1346, May. 1991.

[13] Y. T. Lee, H. D. Seo, A. Kawamura, T. Yamada, Y. Matsumoto, M. Ishida, and T. Nakamura, "Compensation method of offset and its temperature drift in silicon piezoresistive pressure sensor using double wheatstone-bridge configuration," in *Proceedings of the 1995 8th International Conference on Solid-State Sensors and Actuators and Eurosensors IX. Part 1 (of 2)*, 1995, pp. 570–573.

[14] S. Marco, J. Samitier, O. Ruiz, J. Morante, and J. Esteve, "High-performance piezoresistive pressure sensors for biomedical applications using very thin structured membranes," *Measurement science and technology*, vol. 7, no. 9, p. 1195, 1996.

[15] H. Tanigawa, T. Ishihara, M. Hirata, and K. Suzuki, "Mos integrated silicon pressure sensor," *IEEE transactions on Electron Devices*, vol. 32, no. 7, pp. 1191–1195, Jul. 1985.

[16] T. Lisec, M. Kreutzer, and B. Wagner, "Surface micromachined piezoresistive pressure sensors with step-type bent and flat membrane structures," *IEEE Transactions on Electron Devices*, vol. 43, no. 9, pp. 1547–1552, 1996.

[17] C. Malhaire and D. Barbier, "Design of a polysilicon-on-insulator pressure sensor with original polysilicon layout for harsh environment," *Thin solid films*, vol. 427, no. 1-2, pp. 362–366, Mar. 2003.

[18] Y.-T. Lee, H. Takao, and M. Ishida, "Fabrication of high-temperature silicon pressure sensor using sdb-soi technology," *Sensors and Materials*, vol. 17, no. 5, pp. 269–276, 2005.

[19] V. V. Kumar, A. DasGupta, K. Bhat *et al.*, "Process optimization for monolithic integration of piezoresistive pressure sensor and mosfet amplifier with soi approach," *J. Phys. Conf. Ser.*, vol. 34, no. 1, p. 210, Apr. 2006.

[20] K. Sivakumar, N. Dasgupta, K. Bhat, and K. Natarajan, "Sensitivity enhancement of polysilicon piezo-resistive pressure sensors with phosphorous diffused resistors," *J. Phys. Conf. Ser.*, vol. 34, no. 1, pp. 216–219, Apr. 2006.

[21] J. Wang and X. Li, "Single-side fabricated pressure sensors for ic-foundry-compatible, high-yield, and low-cost volume production," *IEEE Electron Device letters*, vol. 32, no. 7, pp. 979–981, Jul. 2011.

[22] H. San, H. Zhang, Q. Zhang, Y. Yu, and X. Chen, "Silicon–glass-based single piezoresistive pressure sensors for harsh environment applications," *Journal of Micromechanics and Microengineering*, vol. 23, no. 7, p. 075020, Jul. 2013.

[23] L. Du, M. Zhang, Z. Zhao, L. Li, C. Liu, Z. Fang, S. Wu, X. Sun, and X. Wang, "A soi-mems atmosphere pressure sensor and its low stress packaging," in *The 9th IEEE International Conference on Nano/Micro Engineered and Molecular Systems (NEMS)*. IEEE, Apr. 2014, pp. 454–457.

[24] S. Zhang, T. Wang, L. Lou, W. M. Tsang, R. Sawada, D.-L. Kwong, and C. Lee, "Annularly grooved diaphragm pressure sensor with embedded silicon nanowires for low pressure application," *Journal of Microelectromechanical Systems*, vol. 23, no. 6, pp. 1396–1407, Dec. 2014.

[25] X. Huang and D. Zhang, "A high sensitivity and high linearity pressure sensor based on a peninsula-structured diaphragm for low-pressure ranges," *Sensors and Actuators A: Physical*, vol. 216, pp. 176–189, Sep. 2014.

[26] K. Singh, R. Joyce, S. Varghese, and J. Akhtar, "Fabrication of electron beam physical vapor deposited polysilicon piezoresistive mems pressure sensor," *Sensors and Actuators A: Physical*, vol. 223, pp. 151–158, Mar. 2015.

[27] J. Wang, R. Chuai, L. Yang, and Q. Dai, "A surface micromachined pressure sensor based on polysilicon nanofilm piezoresistors," *Sensors and Actuators A: Physical*, vol. 228, pp. 75–81, Jun. 2015.

[28] X. Zhao, Y. Yu, D. Li, and D. Wen, "Design, fabrication and characterization of a high-sensitivity pressure sensor based on nano-polysilicon thin film transistors," *AIP Advances*, vol. 5, no. 12, p. 127216, Dec. 2015.

[29] S. S. Kumar and B. Pant, "Polysilicon thin film piezoresistive pressure microsensor: design, fabrication and characterization," *Microsystem Technologies*, vol. 21, no. 9, pp. 1949–1958, Sep. 2015.

[30] J. W. Song, J.-S. Lee, J.-E. An, and C. G. Park, "Design of a mems piezoresistive differential pressure sensor with small thermal hysteresis for air data modules," *Review of Scientific Instruments*, vol. 86, no. 6, p. 065003, Jun. 2015.

[31] G. Liu, W. Cui, H. Hu, F. Zhang, Y. Zhang, C. Gao, and Y. Hao, "Silicon on insulator pressure sensor based on a thermostable electrode for high temperature applications," *Micro & Nano Letters*, vol. 10, no. 10, pp. 496–499, Oct. 2015.

[32] L. Sainan, L. Ting, W. Wei, H. Yingping, Z. Tingli, and X. Jijun, "A novel soi pressure sensor for high temperature application," *Journal of Semiconductors*, vol. 36, no. 1, p. 014014, Jan. 2015.

[33] S. S. Kumar, A. K. Ojha, and B. Pant, "Experimental evaluation of sensitivity and non-linearity in polysilicon piezoresistive pressure sensors with different diaphragm sizes," *Microsystem Technologies*, vol. 22, no. 1, pp. 83–91, Jan. 2016.

[34] C. H. Je, S. Q. Lee, and W. S. Yang, "High sensitivity surface micromachined absolute pressure sensor," *Procedia Engineering*, vol. 168, pp. 725–728, 2016.

[35] S. S. Kumar and B. Pant, "Effect of piezoresistor configuration on output characteristics of piezoresistive pressure sensor: an experimental study," *Microsystem technologies*, vol. 22, no. 4, pp. 709–719, Apr. 2016.

[36] X. Meng and Y. Zhao, "The design and optimization of a highly sensitive and overload-resistant piezoresistive pressure sensor," *Sensors*, vol. 16, no. 3, p. 348, Mar. 2016.

[37] G. Cao, X. Wang, Y. Xu, and S. Liu, "A micromachined piezoresistive pressure sensor with a shield layer," *Sensors*, vol. 16, no. 8, p. 1286, Aug. 2016.

[38] H. Zou, J. Wang, and X. Li, "High-performance low-range differential pressure sensors formed with a thin-film under bulk micromachining technology," *Journal of Microelectromechanical Systems*, vol. 26, no. 4, pp. 879–885, Aug. 2017.

[39] T. Xu, H. Wang, Y. Xia, Z. Zhao, M. Huang, J. Wang, L. Zhao, Y. Zhao, and Z. Jiang, "Piezoresistive pressure sensor with high sensitivity for medical application using peninsula-island structure," *Frontiers of Mechanical Engineering*, vol. 12, no. 4, pp. 546–553, Dec. 2017.

[40] A. V. Tran, X. Zhang, and B. Zhu, "The development of a new piezoresistive pressure sensor for low pressures," *IEEE Transactions on Industrial Electronics*, vol. 65, no. 8, pp. 6487–6496, Aug. 2018.

[41] C. Li, J. Xie, F. Cordovilla, J. Zhou, R. Jagdheesh, and J. L. Ocaña, "Design, fabrication and characterization of an annularly grooved membrane combined with rood beam piezoresistive pressure sensor for low pressure measurements," *Sensors and Actuators A: Physical*, vol. 279, pp. 525–536, Aug. 2018.

[42] D. Burns, "Micromechanical integrated sensors and the planar processed pressure transducer phd thesis university of wisconsin," *Madison, WI, USA*, 1988.

[43] M. Manuvinakurake, U. Gandhi, M. Umapathy, and M. M. Nayak, "Bossed diaphragm coupled fixed guided beam structure for mems based piezoresistive pressure sensor," *Sensor Review*, 2019.

[44] H.-L. Chau and K. Wise, "Noise due to brownian motion in ultrasensitive solid-state pressure sensors," *IEEE transactions on Electron Devices*, vol. 34, no. 4, pp. 859–865, Apr. 1987.

[45] H. Shin, K. Noguchi, and C. Hu, "Thickness and other effects on oxide and interface damage by plasma processing," in *31st Annual Proceedings Reliability Physics 1993*, 1993, pp. 272–279.

[46] G. Li, V. Kilchytska, N. André, L. A. Francis, Y. Zeng, and D. Flandre, "Leakage current and low-frequency noise analysis and reduction in a suspended soi lateral p-i-n diode," *IEEE Transactions on Electron Devices*, vol. 64, no. 10, pp. 4252–4259, Oct. 2017.

Thibault P. Delhaye has received the M.S. degree from the University of Louvain, Louvain-la-Neuve, Belgium in 2015. He is now a PhD candidate student in the Institute of Information and Communication Technologies, Electronics and Applied Mathematics (ICTEAM), University of Louvain. He was Visiting International Research Student at the University of Bristish Columbia, Canada, during fall 2018. His research topic is on highly sensitive and ultra-low-power MEMS pressure sensor based on SOI technology.

Nicolas André (M'09) received the M.S. degrees in electrical engineering from the Louvain School of Engineering, Université Catholique de Louvain (UCL), Louvain-la-Neuve, Belgium, in 2004, and the Ph.D. degree in applied sciences in the field of microelectromechanical systems (MEMS) co-integration from UCL in 2011. From 2011 to 2012, he was with UdeS, Sherbrooke, Canada, as a Post-Doctoral Researcher on bio-inspired methods to improve the LED efficiency. He has co-authored over 100 research papers in international journals and holds two patents. He was a team member in several Walloon, FEDER, and EU projects as CAVIMA, STARFLO+, SHC, FEDER MINATIS, and MICRO+, and FP7 SOI-HITS. His expertise is about microfabrication and sensors (flow, humidity, pressure, light) integrated with SOI CMOS Circuits.

Laurent A. Francis (M.Eng. 2001, Ph.D 2006) is Professor and Head of the Electrical Engineering Department of the Université catholique de Louvain, Belgium. His main focus is on co-integrated, ultra-low power CMOS MEMS sensors for biomedical and environmental applications in the frame of the Internet-of-Things and for harsh environments. He was previously researcher at IMEC in Leuven, Belgium, in the field of acoustic and optical biosensors and piezoelectric RF-MEMS. In 2011, he was visiting professor at the Université de Sherbrooke, Canada. He has authored or co-authored more than 130 research papers in international journals, he is co-editor of two books, and holds five patents. He is board member of the Belgian National Committee Biomedical Engineering. He is a regular member of the IEEE and serves as Treasurer of the IEEE CPMT Benelux Chapter.

Denis Flandre (M'85–SM'03) received the M.S. degree in electrical engineering, and the Ph.D. degree and the Research Habilitation degree from the Université Catholique de Louvain (UCL), Louvain-la-Neuve, Belgium, in 1986, 1990, and 1999, respectively. His doctoral research was on the modeling of silicon-on-insulator MOS devices for characterization and circuit simulation, and his post-doctoral thesis on a systematic and automated synthesis methodology for MOS analog circuits.

He has been a full-time Professor at UCL since 2001. He has authored or co-authored over 1000 technical papers or conference contributions. He received several scientific prizes and best paper awards. He is a co-inventor of 12 patents. He has organized or lectured many short courses on SOI technology, devices and circuits in universities, industrial companies,and conferences. He has participated or coordinated numerous research projects funded by regional and European institutions. He is currently involved in the research and development of SOI MOS devices, digital and analog circuits, and sensors and MEMS for special applications, more specifically high-speed, low-voltage low-power, microwave, biomedical, radiation-hardened, and high-temperature electronics and microsystems.

Prof. Flandre is a Co-Founder of CISSOID, a spin-off company of UCL, focusing on SOI and high-reliability integrated circuit design and products. He is a Scientific Advisor of three other UCL start-ups: INCIZE (semiconductor characterization and modeling for design of digital, analog/RF, and harsh environment applications), e-peas (energy harvesting and processing solutions for longer battery life, increased robustness in all IoT applications) and VOCsens (Volatile Organic Compound smart sensing solutions). He has been a member of several EU Networks of Excellence on High-Temperature Electronics, SOI technology, nanoelectronics and micronanotechnology, and an Active Member of the SOI Industry Consortium and the EUROSOI network.